• Clinical Research •

Enhancing the diagnostic precision of subclinical keratoconus by combining indices from Scheimpflug tomography, corneal biomechanics, and anterior segment optical coherence tomography

Norsyariza Razak[1], Bariah Mohd-Ali[2], Wan Haslina Wan Abdul Halim[1,3]

[1]Department of Ophthalmology, Faculty of Medicine, National University of Malaysia, Cheras 56000, Kuala Lumpur, Malaysia

[2]Optometry and Vision Science Program, Faculty of Health Sciences, National University of Malaysia, Kuala Lumpur 50300, Malaysia

[3]Department of Ophthalmology, Faculty of Medicine and Health Sciences, National UCSI University, Cheras 56000, Kuala Lumpur, Malaysia

Correspondence to: Wan Haslina Wan Abdul Halim. Department of Ophthalmology, Faculty of Medicine, National University of Malaysia, Kuala Lumpur 56000, Malaysia; Faculty of Medicine and Health Sciences, National UCSI University, Kuala Lumpur 56000, Malaysia. afifiyad@yahoo.co.uk

Received: 2025-04-27 Accepted: 2025-12-24

Abstract

● **AIM:** To determine the diagnostic precision of combined Scheimpflug tomography and biomechanical analysis with optical coherence tomography (OCT) for detection of subclinical keratoconus (SCKC).

● **METHODS:** All subjects in this prospective, cross-sectional study underwent Scheimpflug tomography (Pentacam HR), air-puff tonometry (Corvis ST), and spectral-domain optical coherence tomography (Cirrus HD SD-OCT). The diagnosis of SCKC and keratoconus (KCN) were based on the Oculus Pentacam classification. Combined diagnostic models were developed using stepwise logistic regression (SLR). The Kruskal-Walli's test evaluated group differences. Diagnostic accuracy was assessed by calculating the area under the curve (AUC).

● **RESULTS:** A total of 137 participants comprising 73 females and 64 males, including 48 with KCN, 36 with SCKC, and 53 with normal corneas. The mean age for each group was 31.39±10.82y, 29.25±7.33y, and 30.45±8.03y, respectively. Most examined tomography, biomechanical, and pachymetry indices showed significant differences between KCN, SCKC, and normal eyes (P<0.05). Single tomographic biomechanical index (TBI) data was the most effective in identifying SCKC, achieving an AUC of 0.978 (P<0.001) with 100% sensitivity and 84.91% specificity. Combining SD-OCT and Pentacam HR data, the SLR model yielded superior accuracy for SCKC detection, with an AUC of 0.966 (86.11% sensitivity and 96.13% specificity). The highest accuracy for SCKC identification was attained by integrating data from all three devices, resulting in 0.990 accuracy (91.67% sensitivity; 100% specificity).

● **CONCLUSION:** While current parameters accurately identify KCN, they are less effective for SCKC. Integrating Scheimpflug-based biomechanical and tomographic analysis with SD-OCT improves SCKC detection, supporting more accurate screening and earlier identification in patients with otherwise normal findings.

● **KEYWORDS:** keratoconus; subclinical keratoconus; Oculus Pentacam; Oculus Corvis ST; optical coherence tomography

DOI:10.18240/ijo.2026.07.08

Citation: Razak N, Mohd-Ali B, Halim WHWA. Enhancing the diagnostic precision of subclinical keratoconus by combining indices from Scheimpflug tomography, corneal biomechanics, and anterior segment optical coherence tomography. *Int J Ophthalmol* 2026;19(7):1284-1292

INTRODUCTION

Identifying subclinical keratoconus (SCKC) is essential, particularly for individuals contemplating refractive surgery. Undiagnosed SCKC substantially elevates the likelihood of post-surgical complications, including corneal ectasia. Research has demonstrated that specific measurements obtained from topographic and tomographic evaluations can effectively distinguish between healthy corneas and those affected by SCKC[1]. Over the past decade, major advances in corneal imaging have transformed ectasia screening. Imaging modalities, such as corneal topography, optical coherence tomography (OCT), corneal biomechanics, anterior segment

OCT, and confocal microscopy, can optimize the diagnosis of early and forme fruste keratoconus[2].

Scheimpflug tomography (Pentacam HR), offers detailed anterior and posterior corneal maps, pachymetry, and elevation data, facilitating the detection of subtle corneal shape changes not discernible through topography alone[3]. Nevertheless, these parameters from Pentacam can nonetheless exhibit considerable overlap between normal eyes and those in the earliest stages of keratoconus (KCN)[4-5]. Previous studies have highlighted a reduction in corneal biomechanical strength as a key factor in the emergence of KCN[6], and can be used to detect changes in the mechanical properties of the cornea before significant surface changes occur[7]. By combining Pentacam parameters with Corvis ST-derived biomechanics, the tomographic biomechanical index (TBI), along with the Corvis biomechanical index (CBI), has proven to be a highly effective tool for identifying early ectasia[8-10]. However, despite their strong diagnostic performance, some ambiguous or borderline cases remain challenging to distinguish[7].

High-resolution spectral-domain OCT (SD-OCT) provides detailed mapping of the corneal epithelium and stroma. Epithelial remodelling, acting as a compensatory mechanism that can obscure incipient stromal changes, has emerged as a key indicator of SCKC[11-12]. Despite these advantages, SD-OCT has limitations. Its assessment is typically restricted to the central cornea, potentially missing peripheral or paracentral changes[13]. SD-OCT also does not measure biomechanical properties, which may decline before morphological alterations occur, however when the epithelial mapping combined with biomechanical parameters, may further enhance early detection[10].

Multimodal imaging is instrumental in offering a thorough evaluation of both KCN and SCKC, encompassing diagnosis, classification, staging, prognosis, personalized treatment planning, and clinical follow-up[14-16]. Machine learning models that integrate tomographic and biomechanical data have achieved sensitivities and specificities around 90%, highlighting the value of integrated approaches[17]. Combining the latest technology with traditional techniques is expected to be a future trend to improve the early diagnosis of KCN[18]. Because SCKC encompasses structural, biomechanical, and microarchitectural corneal changes, singular imaging methods may fail to detect early disease. Combining Scheimpflug tomography with corneal biomechanical indices and SD-OCT-based epithelial and stromal metrics provides a multimodal approach that can improve diagnostic performance and identify subclinical ectasia sooner. By applying stepwise logistic regression to generate optimized multimodal predictors, we aim to determine whether integrating complementary imaging modalities provides superior sensitivity and specificity compared with single-platform parameters. Advancing the precision of SCKC detection would have substantial implications for refractive surgery screening, early disease management, and prevention of ectasia-related vision loss.

PARTICIPANTS AND METHODS

Ethical Approval This research was approved by the National University of Malaysia Ethics Committee with reference code (JEP-2021-654) and funded by the Fundamental Grant of the Faculty of Medicine, National University of Malaysia with reference code (FF-2021-374).

Study Design & Participants This cross-sectional prospective study enrolled 137 subjects (KCN: 48, SCKC 36 and 53 normal healthy as control. The recruitment started from December 2022 to June 2024 in Hospital Canselor Tuanku Muhriz UKM. Written informed consent was obtained from all the subjects. All the participants were divided into three groups: the definite KCN group, the SCKC group, and the control group. The clinical diagnosis of KCN was based on slit-lamp findings (*i.e.*, stromal thinning, conical protrusion of the corneal apex, Fleischer rings, Vogt striae, or anterior stromal scars), and the presence of abnormal topographic patterns on the sagittal front curvature map[19], disregarding tomographic and biomechanical findings, and was confirmed by the ophthalmologist. SCKC eyes were diagnosed according to the following criteria: 1) Normal-appearing cornea on slit-lamp bio microscopy, keratometry, retinoscopy, and ophthalmoscopy; 2) Inferior-superior asymmetry and/or bow-tie pattern with skewed radial axes; 3) No history of contact lens use, ocular surgery, or trauma; 4) Diagnosis of KCN in the fellow eye[20]. The following are the exclusion criteria: previous ocular surgery or trauma, significant corneal scarring or associated ocular pathology. Participants who did not abstain from wearing soft contact lenses for 2wk or rigid gas permeable (RGP) lenses for 4wk prior to the examinations were excluded.

Procedure & Data Collection All the participants underwent basic eye examinations, including visual acuity, slit-lamp examination and refraction. Furthermore, the following parameters were assessed using the Oculus Pentacam HR (Wetzlar, Germany). For corneal topography and tomography: keratometry in the flat/steep meridian (K1/K2), maximal keratometry (Kmax), thinnest point pachymetry (TP), central corneal thickness (CCT), front elevation at the thinnest point (F.Ele.Th), back elevation at the thinnest point (B.Ele.Th), maximum Ambrósio relational thickness (ARTmax), Pentacam random forest index (PRFI), Belin/Ambrósio enhanced ectasia display (BAD), index of surface variance (ISV), index of vertical asymmetry (IVA), keratoconus index (KI), inferior-superior index (I-S), index of height asymmetry (IHA), index of height decentration (IHD), minimum radius of curvature

(Rmin), and inferior-superior astigmatism index (KISA). The biomechanical parameters collected by the Oculus Corvis ST (Wetzlar, Germany), were included the time until the first/second applanation (A1T/A2T), velocity of the corneal apex during the first or second applanation (A1V/A2V), length at the first/second applanation (A1L/A2L), corneal deflection amplitude at the moment of the highest concavity deformation amplitude (HCDA), peak distance at the highest concavity (HCPD), central concave curvature at the highest concavity (HCR), maximum deformation amplitude (DA), CCT, deformation amplitude ratio max 2 mm (DA ratio), integrated radius (IR), Ambrósio relational thickness horizontal (ARTh), stiffness parameter at A1 (SPA1), CBI, and TBI. The parameters measured using Cirrus anterior segment OCT (Dublin, California, United States) were, pachymetry thickness map 2–5 mm for minimal (Min), average (Avg), maximal (Max), superior-inferior (S-I), superonasal-inferotemporal (SNIT), and epithelium thickness map 2–5 mm for Min, Avg, Max, S-I, SNIT.

Statistical Analysis Statistical analysis was conducted using IBM SPSS (version 27.0) and MedCalc (version 22.030). The Shapiro-Wilk test assessed the normality of corneal parameters. Normally distributed data were compared using one-way analysis of variance (ANOVA) followed with pairwise Bonferroni test; non-normally distributed data used the Kruskal-Walli's test followed with pairwise Dunn test. All tests were one-tailed with $P<0.05$ considered significant. Receiver operating characteristic (ROC) curves were utilised to demonstrate the sensitivity and specificity of various cut-off points for multimodal imaging parameters in KCN, SCKC, and control eyes. Additionally, the optimal cut-off value, the area under the curve (AUC), and the Youden index were established. A value of 1.0 for AUC signifies perfect discrimination, while values less than 0.5 indicate that the assessed parameter lacks diagnostic ability. To compare the AUC pairwise, the De Long test was employed. Parameters with AUC value exceeding 0.8 from all three multimodal imaging devices will be analysed using stepwise binary Logistic regression analysis (SLR) to identify the most predictive model for the diagnosis of SCKC. The Hosmer-Lemeshow test was used to evaluate the goodness-of-fit of the SLR models. All variables were initially included in the model and subsequently removed based on significance. The new model was compared to the previous one; if no significant differences were found, the simplest model with the lowest Akaike Information Criterion (AIC) value, minimal collinearity (below 2), and optimal goodness of fit was chosen. The proposed model will be re-evaluated using ROC curve analysis to determine the AUC, sensitivity, and specificity. SLR proposed model was built with combined parameters from 1) Oculus Pentacam HR only; 2) Oculus Corvis ST only; 3) Cirrus 5000 anterior segment OCT; 4) combined Oculus Pentacam HR, Oculus Corvis ST, and Cirrus 5000 anterior segment OCT.

RESULTS

Comparison of Multimodal Imaging in Subclinical Keratoconus, Keratoconus, and Normal A total of 137 participants were assessed, including 48 with KCN, 36 with SCKC, and 53 with normal corneas. The mean age for each group was 31.39±10.82, 29.25±7.33, and 30.45±8.03y, respectively. There was no significant difference in age among the three groups (SCKC, KCN, and normal) with a $P>0.05$. Furthermore, there were significant differences in all three multimodal imaging parameters between the groups with a $P<0.001$. Pairwise comparisons showed significant differences in all Oculus Pentacam HR parameters between the SCKC and KCN groups ($P<0.05$). Additionally, there were significant differences ($P<0.05$) between the SCKC and normal groups in all parameters except for K1 and K2. Significant differences were also observed in all corneal biomechanical parameters using Oculus Corvis ST between the SCKC and normal groups, except for A1L, A2L, and A2T with a $P>0.05$. Furthermore, there were significant differences ($P<0.001$) in Cirrus anterior segment OCT parameters between the groups, except for epithelium thickness map (Avg) with a P value of 0.265. Additionally, significant differences were observed in Cirrus OCT Pachymetry parameters between the SCKC and normal groups, except for epithelial thickness map (Avg) and (Max) and pachymetry map (SNIT) with a P value of >0.05. These comparisons are shown in Figure 1.

Diagnostic Ability of Multimodal Imaging in Differentiating Subclinical Keratoconus from Normal Eyes The diagnostic capabilities of eight Oculus Pentacam HR parameters for detecting SCKC in the normal population were generally strong, with an AUC of over 0.80. The PRFI has demonstrated as the highest SCKC predictive model with an AUC of 0.975. The PRFI is a novel shape index developed using a random forest machine learning algorithm based on multiple Pentacam parameters. It is designed to improve the detection of KCN, including in SCKC[21]. The BAD demonstrated the second highest predictive model, with an AUC of 0.935. It is a multivariate index derived from a combination of anterior and posterior corneal elevation data and pachymetry (corneal thickness) data. It is part of the BAD, which integrates these parameters to provide a comprehensive assessment of corneal shape and detect ectasia diseases such as KCN[22]. Additionally, the ISV showed an AUC of 0.906. The ISV measures how much the corneal radius deviates from the average value. Elevated ISV values are typically found in instances of irregular astigmatism. In essence, the ISV quantifies the irregularity of the surface curvature[23]. The

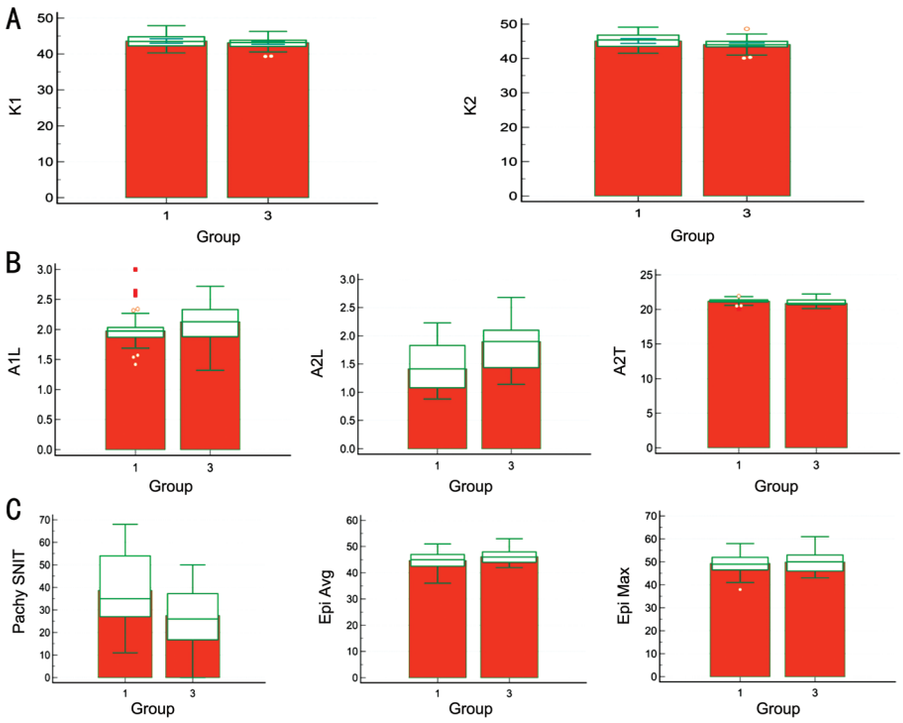

Figure 1 Comparison of corneal imaging parameters between subclinical keratoconus and normal groups (*P*>0.05) Oculus Corvis ST parameters in subclinical keratoconus (group 1) *vs* normal (group 3), no significant different in K1 and K2 (A), A1L, A2L, and A2T (B), and pachy SNIT, Epi Avg, and Epi Max (C). SNIT: Superonasal-inferotemporal; K1: Keratometry in the flat meridian; K2: Keratometry in the steep meridian; A1L: Length at the first applanation; A2L: Length at the second applanation; A2T: Time until the second applanation.

overall findings are shown in Table 1. In contrast, only four Oculus Corvis ST parameters were found to be effective in differentiating between SCKC and normal eyes, with an AUC above 0.80. The following results are presented in Table 2. TBI showed the highest diagnostic ability with an AUC of 0.978, followed by CCT with an AUC of 0.846. The TBI index was developed through a robust and innovative integration of data obtained from Scheimpflug-based corneal tomographic and biomechanical analyses[8]. For anterior segment pachymetry Cirrus OCT, only Min and Avg from the pachymetry thickness map (2–5 mm) demonstrated diagnostic ability with an AUC above 0.80. Min (pachymetry thickness map 2–5) showed the highest predictive model, with an AUC of 0.921, for detecting SCKC in normal individuals. The overall findings are being shown in Table 3. In general, the Oculus Pentacam showed better performance in distinguish SCKC compared to the other two devices.

Stepwise Logistic Regression Predicted Model of Combined Multimodal Imaging to Detect Subclinical Keratoconus The results from the combined model of Oculus Pentacam HR parameters, which included BAD, CCT, and TP, were statistically significant with a χ^2 value of 78.440 and a P<0.001. This combined model can effectively distinguish between individuals with and without SCKC in a normal population. The model showed an AUC of 0.961 with a 95% confidence interval of 0.897–0.990 and a standard error of 0.017. It also had a sensitivity of 83.3% and a specificity of 98.1%. However, stepwise logistic regression on Oculus Corvis ST parameters only identified TBI as a significant predictor for SCKC, with a χ^2 value of 88.830 and a P<0.0001. This model had an AUC of 0.978. In addition, for Carl Zeiss Cirrus Anterior Segment Pachymetry parameters, the combined model of Min (Pachymetry 2–5) and Min (Epithelium 2–5) was statistically significant with a χ^2 value of 71.144 and a P<0.001. This model had an AUC of 0.961 with a 95% confidence interval of 0.897–0.890 and a standard error of 0.024. It also had a sensitivity of 83.3% and a specificity of 98.1%. Furthermore, the predicted model from the three multimodal imaging techniques, which included TBI from Oculus Corvis ST and Min (Pachymetry 2–5) from Carl Zeiss Cirrus Anterior Segment Pachymetry, was statistically significant with a χ^2 value of 99.744 and a P<0.001. This model had an AUC of 0.990 with a 95% confidence interval of 0.941–1.00 and a standard error of 0.007. It also had a sensitivity of 91.67% and a specificity of 100%. Table 4 presented the comparison of diagnostic ability in AUC, sensitivity, and specificity for each predicted model.

DISCUSSION

Previous studies have shown significant differences in corneal thickness, volume, and elevation between SCKC and healthy eyes, particularly using advanced topographic and tomographic techniques[3,5,24]. In this study, nearly all

Table 1 Receiver operating characteristic curve (ROC) analysis of Oculus Pentacam parameters for KCN and SCKC *vs* normal

Pentacam parameters	SCKC *vs* normal AUC (95%CI)	*P*	KCN *vs* normal AUC (95%CI)	*P*
ISV	0.906 (0.826–0.958)	<0.001	1.00 (0.964–1.00)	<0.001
IVA	0.864 (0.775–0.928)	<0.001	0.999 (0.962–1.00)	<0.001
IHA	0.670 (0.562–0.766)	0.007	0.892 (0.819–0.945)	<0.001
IHD	0.837 (0.744–0.907)	<0.001	0.999 (0.963–1.00)	<0.001
KI	0.725 (0.620–0.814)	0.003	1.00 (0.964–1.00)	<0.001
I-S	0.685 (0.578–0.780)	0.004	0.978 (0.927–0.997)	<0.001
KISA	0.740 (0.637–0.828)	<0.001	0.990 (0.946–1.00)	<0.001
Rmin	0.693 (0.586–0.787)	0.001	0.981 (0.932–0.998)	<0.001
K1	0.558 (0.448–0.663)	0.368	0.873 (0.792–0.931)	<0.001
K2	0.651 (0.543–0.749)	0.018	0.977 (0.925–0.997)	<0.001
Kmax	0.698 (0.591–0.791)	0.014	0.994 (0.952–1.00)	<0.001
CCT	0.846 (0.754–0.914)	<0.001	0.976 (0.923–0.996)	<0.001
TP	0.864 (0.775–0.928)	<0.001	0.982 (0.933–0.998)	<0.001
F.Ele.Th	0.796 (0.698–0.874)	<0.001	0.998 (0.961–1.00)	<0.001
B.Ele.Th	0.810 (0.713–0.885)	<0.001	0.997 (0.958–1.00)	<0.001
ARTmax	0.856 (0.766–0.922)	<0.001	0.981 (0.931–0.998)	<0.001
BAD	0.935 (0.862–0.976)	<0.001	1.00 (0.964–1.00)	<0.001
PRFI	0.975 (0.920–0.997)	<0.001	1.00 (0.978–1.00)	<0.001

AUC: Area under the curve; CI: Confidence interval; SCKC: Subclinical keratoconus; KCN: Keratoconus; ISV: Index surface variability; IVA: Index of vertical asymmetry; IHA: Index of height asymmetry; IHD: Index of height decentration; KI: Keratoconus index; I-S: Inferior-superior difference value; KISA: Keratometry inferior-superior and astigmatism index; Rmin: Minimum radius of curvature; K1: Flat keratometry; K2: Step keratometry; Kmax: Maximum keratometry; CCT: Central corneal thickness; TP: Thinnest pachymetry; F.Ele.Th: Front elevation at the thinnest location; B.Ele.Th: Back elevation at the thinnest location; ARTmax: Ambriosio relational thickness maximum; BAD: Belin-Ambrósio enhanced ectasia display; PRFI: Pentacam random forest index.

Table 2 Receiver operating characteristic curve (ROC) analysis of Oculus Corvis ST for KCN and SCKC *vs* normal groups

Corvis ST parameters	SCKC *vs* normal AUC (95%CI)	*P*	KCN *vs* normal AUC (95%CI)	*P*
CBI	0.748 (0.645–0.834)	<0.001	0.999 (0.963–1.00)	<0.001
TBI	0.978 (0.922–0.997)	<0.001	1.00 (0.964–1.00)	<0.001
CCT	0.866 (0.777–0.929)	<0.001	1.00 (0.964–1.00)	<0.001
ARTh	0.643 (0.534–0.741)	0.017	0.974 (0.921–0.995)	<0.001
SPA1	0.794 (0.695–0.872)	<0.001	0.982 (0.932–0.998)	<0.001
DA	0.795 (0.696–0.873)	<0.001	0.928 (0.859–0.970)	<0.001
IR	0.846 (0.754–0.914)	<0.001	0.972 (0.919–0.995)	<0.001
A1L	0.619 (0.510–0.720)	<0.001	0.808 (0.717–0.879)	<0.001
A2L	0.741 (0.637–0.828)	<0.001	0.745(0.649–0.827)	<0.001
A1V	0.723 (0.618–0.813)	<0.001	0.846 (0.760–0.910)	<0.001
A2V	0.695 (0.588–0.788)	<0.001	0.825 (0.737–0.894)	<0.001
A1T	0.800 (0.701–0.877)	<0.001	0.898 (0.821–0.949)	<0.001
A2T	0.639 (0.530–0.738)	<0.001	0.745 (0.649–0.827)	<0.001
HCPD	0.742 (0.638–0.829)	<0.001	0.689 (0.588–0.778)	<0.001
HCR	0.781 (0.681–0.862)	<0.001	0.927 (0.858–0.970)	<0.001
HCDA	0.792 (0.693–0.871)	<0.001	0.889 (0.821–0.949)	<0.001

AUC: Area under the curve; CI: Confidence interval; SCKC: Subclinical keratoconus; KCN: Keratoconus; CBI: Corvis biomechanical index; TBI: Tomographic biomechanical index; CCT: Central corneal thickness; ARTh: Ambrosio relational thickness horizontal; SPA1: Stiffness parameter at the first applanation; DA: Deformation amplitude ratio at 2 mm; IR: Integrated radius; A1L: First applanation length; A2L: Second applanation length; A1V: Applanation-1 velocity; A2V: Applanation-2 velocity; A1T: The time until the first applanation; A2T: The time until the second applanation; HCPD: Highest concavity peak distance; HCR: Highest concavity radius; HCDA: Highest concavity deformation amplitude.

Table 3 Receiver operating characteristic curve (ROC) analysis of Cirrus OCT pachymetry map parameters for KCN and SCKC *vs* normal groups

Pachymetry parameters	SCKC *vs* normal AUC (95%CI)	*P*	KCN *vs* normal AUC (95%CI)	*P*
Pachymetry thickness map (2-5 mm)				
Min	0.921 (0.845-0.968)	<0.001	1.00 (0.964-1.00)	<0.001
Avg	0.863 (0.774-0.927)	<0.001	0.962 (0.904-0.990)	<0.001
Max	0.756 (0.653-0.840)	<0.001	0.874 (0.793-0.932)	<0.001
SI	0.652 (0.544-0.750)	0.011	0.798 (0.706-0.871)	<0.001
SNIT	0.636 (0.528-0.736)	0.030	0.835 (0.747-0.901)	<0.001
Epithelium thickness map (2-5 mm)				
Min	0.675 (0.567-0.770)	0.003	0.893 (0.816-0.946)	<0.001
Avg	0.609 (0.500-0.711)	0.074	0.565 (0.463-0.664)	0.272
Max	0.515 (0.664-0.810)	0.808	0.738 (0.641-0.820)	<0.001
SI	0.652 (0.544-0.750)	0.020	0.739 (0.642-0.822)	<0.001
SNIT	0.664 (0.556-0.761)	0.008	0.719 (0.621-0.804)	<0.001

AUC: Area under the curve; CI: Confidence interval; SCKC: Subclinical keratoconus; KCN: Keratoconus; Min: Minimum; Avg: Average; Max: Maximum; SI: Superior-inferior; SNIT: Superonasal inferotemporal.

Table 4 Comparison of area under the curve (AUC), sensitivity, and specificity analyses of multimodal imaging predicted models to detect subclinical keratoconus

Logistic regression model	AUC (95%CI)	*P*	Sensitivity	Specificity
Oculus Pentacam, Corvis ST & Cirrus OCT	0.990 (0.941–1.00)	<0.001	91.67	100
Oculus Pentacam & Cirrus OCT	0.966 (0.905–0.993)	<0.001	86.11	96.13
Oculus Pentacam	0.961 (0.897–0.990)	<0.001	83.30	98.10
Oculus Corvis ST	0.978 (0.922–0.997)	<0.001	100	84.91
Cirrus OCT	0.943 (0.833–0.957)	<0.001	83.33	96.23

CI: Confidence interval; OCT: Optical coherence tomography.

tomographic and pachymetry parameters differed significantly (P<0.05), except K1 and K2, whereas earlier reports noted differences across all parameters[4,25]. Corneal biomechanics also differed significantly between SCKC and controls, except for A1L, A2L, and A2T. These findings align with Koc *et al*[24], who reported significant discrepancies in A2L, A1V, A2V, and TBI, and Ren *et al*[26], who identified SPA1 and CBI as discriminative. Peyman *et al*[9] also highlighted differences in DA ratio, TBI, CBI, ARTh, and SPA1. Additionally, SD-OCT parameters revealed notable changes in SCKC eyes, consistent with Ostadian *et al*[27], who reported reductions in epithelial thickness maps (SI, SNIT), and Yang *et al*[11], who observed differences in pachymetry (Min, Avg, SNIT).

In this study, PRFI outperformed BAD in discriminating SCKC from normal eyes, consistent with previous reports[28-30], although BAD has also shown utility in earlier studies[4-5,25]. The TBI parameter from Corvis ST demonstrated the highest predictive value, with an AUC of 0.978, aligning with prior findings reporting AUCs of 0.925–0.960[9,21,25,31]. Additionally, the minimum pachymetry (2–5 mm) achieved an AUC of 0.921, exceeding earlier reports by Salman *et al*[32] (0.750) and Heidari *et al*[14] (0.782), highlighting the enhanced sensitivity of these metrics for SCKC detection.

While standard corneal topography may suffice for diagnosing overt KCN, a combination of variables is recommended to improve detection of SCKC. In this study, a model incorporating BAD, CCT, and TP demonstrated superior diagnostic performance with an AUC of 0.961. Previous studies have similarly highlighted the value of multivariable approaches; Hashemi *et al*[33] reported that a logistic regression model combining BAD, IVA, ISV, and fifth-order vertical coma achieved 83.6% sensitivity and 96.9% specificity, while another model using TP, anterior coma at 90°, and posterior coma at 90° achieved 97.6% sensitivity and 98.8% specificity[18]. In our stepwise logistic regression, TBI emerged as the most discriminative single parameter from Corvis ST (AUC 0.978). Comparatively, Shiga *et al*[34] reported an AUC of 0.938 using A1V and SPAI, and Peña-García *et al*[35] identified DA, A1T, and CCT as optimal discriminators with an AUC of 0.893. The combined model from this study using anterior segment SD-OCT parameters proposed the combination of minimum pachymetry and epithelial thickness maps achieved an AUC of 0.943, closely aligning with prior studies reporting AUCs of 0.950 and 0.893[34,36].

Early identification of SCKC is essential due to its risk of progression and its implications for refractive surgery screening. In this study, the multimodal stepwise logistic regression model combining TBI (Corvis ST) and minimum

Table 5 Summary of combined multimodal imaging for subclinical keratoconus detection from the previous studies

Combinations	Sensitivity	Specificity	Area under the curve (AUC)
Combined Oculus Pentacam parameters			
This study (BAD, CCT, and TP)	0.833	0.981	0.961
Castro-Luna *et al*[18]	0.75	0.963	0.920
Hashemi *et al*[41]	0.836	0.969	NA
Zhang *et al*[42]	0.610	0.725	0.713
Combined Oculus Corvis ST parameters			
This study (TBI)	1.00	0.849	0.978
Shiga *et al*[34]	0.869	0.829	0.938
Zhang *et al*[42]	0.632	0.886	0.811
Peña-García *et al*[35]	0.857	0.820	0.893
Combined OCT parameters			
This study (Min pachy & Min Epi)	0.833	0.962	0.943
Shiga *et al*[34], Optovue OCT	0.826	0.942	0.893
Saad *et al*[36]	0.75	0.985	0.950
Yang *et al*[11]	1.00	1.00	1.00
Combined 2 devices			
This study (Pentacam & Cirrus)	0.861	0.961	0.966
Song *et al*[38], Pentacam & Corvis	0.897	0.943	0.922
Ren *et al*[26], Pentacam & Corvis	0.769	0.904	0.909
Zhang *et al*[40], Pentacam & Corvis	1.00	0.84	0.965
Shiga *et al*[34], Corvis & Optovue	0.913	0.903	0.947
Zhang *et al*[42], Pentacam & Corvis	0.754	0.871	0.849
Pérez-Rueda *et al*[17], Pentacam & Corvis	0.895	0.967	0.949
Wallace *et al*[43], Pentacam & Corvis	1.00	1.00	1.00
Combined 3 devices			
This study, Pentacam & Corvis & Cirrus	0.916	1.00	0.990

CCT: Central corneal thickness; TP: Thinnest pachymetry; BAD: Belin-Ambrósio enhanced ectasia display; TBI: Tomographic biomechanical index; Min Pachy: Minimum pachymetry thickness map; Min Epi: Minimum epithelial thickness map; OCT: Optical coherence tomography; NA: Not available.

pachymetry (2–5 mm) from SD-OCT achieved excellent diagnostic performance (AUC 0.990), underscoring the value of integrating complementary imaging modalities. This is consistent with a recent systematic review by Hashemi *et al*[37], which demonstrated high pooled accuracy of artificial intelligence (AI)-based Pentacam models for SCKC detection and reported pooled accuracy estimates of 99.2%–99.0% when Scheimpflug and Placido imaging were combined with biomechanical and wavefront analyses; the Pentacam system alone achieved a pooled estimate accuracy of 92.25%. In another study, Pérez-Rueda *et al*[17] proposed a diagnostic model for SCKC using Oculus Pentacam, ARTh, and A2V from Oculus Corvis ST, resulting in 89.5% sensitivity, 96.7% specificity, and an AUC of 0.951. While Song *et al*[38] utilized decision tree models with classification and regression tree (CART) algorithms, including BAD, back eccentricity (Becc), maximum pachymetric progression index from Pentacam, and SPA1 from Corvis ST, achieving an AUC of 0.922. Other predictive model proposed corneal hysteresis (CH) from Ocular Response Analyzer (ORA) and BAD index from Oculus Pentacam, with an AUC of 0.948, 87.1% sensitivity, and 91.4% specificity[39]. Another stepwise logistic regression model proposed the combined F.Ele.Th from Oculus Pentacam, HCDA, and SPA1 from Corvis ST with an AUC of 0.965 for distinguishing forme fruste KCN from normal[40]. Table 5 summarizes the previous study's accuracy, sensitivity, and specificity to detect SCKC by using combined parameters and combined devices.

The lack of standardised terminology for SCKC creates confusion, with various terms such as "KCN suspect" and "forme fruste KCN" being used. This inconsistency in the nomenclature impedes the establishment of widely accepted diagnostic criteria and protocols. This research may also be limited by its small sample size and the fact that it was conducted at a single centre. However, sample size in our study exceeds the required threshold and is appropriately aligned with the study's objectives, reflecting the demographic characteristics of the KCN population in Malaysia. The

Malaysian population is characterized by its unique diversity, comprising a multi-ethnic predominantly consisting of three major ethnic groups: Malays, Chinese, and Indians. To mitigate potential bias, operator standardization and technical validation have been rigorously applied in this study.

In summary, most Pentacam HR-derived parameters demonstrated stronger overall performance for identifying SCKC compared with indices obtained from the Corvis ST and Cirrus 5000 OCT. Nonetheless, the TBI remained the single most accurate predictor of SCKC. Importantly, our findings show that integrating corneal tomography, biomechanics, and pachymetry profiling through multimodal imaging substantially enhances diagnostic precision. The combined model incorporating TBI and minimum pachymetry (2–5 mm) emerged as a particularly robust predictor for detecting SCKC in the general population.

The rapid evolution of KCN diagnostics from early topographic methods to contemporary machine learning approaches is undeniable. AI and machine learning algorithms now consistently achieve sensitivities and specificities exceeding 90% for SCKC detection, outperforming traditional indices[44]. The integration of multimodal imaging with AI-driven analytics offers the potential for real-time, point-of-care decision support within routine clinical workflows. Beyond early diagnosis, machine learning holds promise for enhancing individualized KCN management, including optimizing contact lens fitting, guiding corneal cross-linking strategies, refining intracorneal ring segments (ICRS) implantation planning, improving refractive surgery screening, and informing phakic intraocular lens (IOL) sizing and keratoplasty selection. Collectively, these advances underscore the transformative potential of combined multimodal imaging and AI in reshaping the early detection and management of KCN.

ACKNOWLEDGEMENTS

Foundation: Supported by the Faculty of Medicine National University of Malaysia (UKM).

Conflicts of Interest: Razak N, None; **Mohd-Ali B,** None; **Halim WHWA,** None.

REFERENCES

1 Henriquez MA, Hadid M, Izquierdo L Jr. A systematic review of subclinical keratoconus and forme fruste keratoconus. *J Refract Surg* 2020;36(4):270-279.

2 Al Bdour M, Sabbagh HM, Jammal HM. Multi-modal imaging for the detection of early keratoconus: a narrative review. *Eye Vis (Lond)* 2024;11(1):18.

3 Koc M, Tekin K, Kiziltoprak H, *et al*. Topometric and tomographic evaluation of subclinical keratoconus. *Ophthalmic Epidemiol* 2020;27(4):289-297.

4 Huseynli S, Abdulaliyeva F. Evaluation of scheimpflug tomography parameters in subclinical keratoconus, clinical keratoconus and normal Caucasian eyes. *Turk J Ophthalmol* 2018;48(3):99-108.

5 Toprak İ, Martin Ç, Güneş CE, *et al*. Revisiting pentacam parameters in the diagnosis of subclinical and mild keratoconus based on different grading system definitions. *Turk J Ophthalmol* 2023;53(6):324-335.

6 Falgayrettes N, Patoor E, Cleymand F, *et al*. Biomechanics of keratoconus: Two numerical studies. *PLoS One* 2023;18(2):e0278455.

7 Komninou MA, Seiler TG, Enzmann V. Corneal biomechanics and diagnostics: a review. *Int Ophthalmol* 2024;44(1):132.

8 Ambrósio R Jr, Lopes BT, Faria-Correia F, *et al*. Integration of scheimpflug-based corneal tomography and biomechanical assessments for enhancing ectasia detection. *J Refract Surg* 2017;33(7):434-443.

9 Peyman A, Sepahvand F, Pourazizi M, *et al*. Corneal biomechanics in normal and subclinical keratoconus eyes. *BMC Ophthalmol* 2023;23(1):459.

10 Wang XR, Maeno S, Wang YX, *et al*. Early diagnosis of keratoconus using corneal biomechanics and OCT derived technologies. *Eye Vis (Lond)* 2025;12(1):18.

11 Yang YL, Pavlatos E, Chamberlain W, *et al*. Keratoconus detection using OCT corneal and epithelial thickness map parameters and patterns. *J Cataract Refract Surg* 2021;47(6):759-766.

12 Yücekul B, Dick HB, Taneri S. Systematic detection of keratoconus in OCT: corneal and epithelial thickness maps. *J Cataract Refract Surg* 2022;48(12):1360-1365.

13 Wang ZZ, Dong RL, Yuan YF, *et al*. The role of corneal epithelial thickness map in detecting early keratoconus. *Graefes Arch Clin Exp Ophthalmol* 2025;263(4):1035-1044.

14 Heidari Z, Mohammadpour M, Hajizadeh F, *et al*. Corneal layer thickness in keratoconus using optical coherence tomography. *Clin Exp Optom* 2024;107(1):32-39.

15 Ambrósio R, Salomão MQ, Barros L, *et al*. Multimodal diagnostics for keratoconus and ectatic corneal diseases: a paradigm shift. *Eye Vis (Lond)* 2023;10(1):45.

16 Alqudah N. Keratoconus: imaging modalities and management. *Med Hypothesis Discov Innov Ophthalmol* 2024;13(1):44-54.

17 Pérez-Rueda A, Jiménez-Rodríguez D, Castro-Luna G. Diagnosis of subclinical keratoconus with a combined model of biomechanical and topographic parameters. *J Clin Med* 2021;10(13):2746.

18 Castro-Luna G, Jiménez-Rodríguez D, Castaño-Fernández AB, *et al*. Diagnosis of subclinical keratoconus based on machine learning techniques. *J Clin Med* 2021;10(18):4281.

19 Mas Tur V, MacGregor C, Jayaswal R, *et al*. A review of keratoconus: Diagnosis, pathophysiology, and genetics. *Surv Ophthalmol* 2017;62(6):770-783.

20 de Sanctis U, Aragno V, Dalmasso P, *et al*. Diagnosis of subclinical keratoconus using posterior elevation measured with 2 different methods. *Cornea* 2013;32(7):911-915.

21 Liu Y, Zhang Y, Chen YG. Application of a scheimpflug-based biomechanical analyser and tomography in the early detection of subclinical keratoconus in Chinese patients. *BMC Ophthalmol* 2021;21(1):339.

22 Motlagh MN, Moshirfar M, Murri MS, *et al*. Pentacam® corneal tomography for screening of refractive surgery candidates: a review of the literature, part I. *Med Hypothesis Discov Innov Ophthalmol* 2019;8(3):177-203.

23 Doctor K, Vunnava KP, Shroff R, *et al*. Simplifying and understanding various topographic indices for keratoconus using Scheimpflug based topographers. *Indian J Ophthalmol* 2020;68(12):2732-2743.

24 Koc M, Aydemir E, Tekin K, *et al*. Biomechanical analysis of subclinical keratoconus with normal topographic, topometric, and tomographic findings. *J Refract Surg* 2019;35(4):247-252.

25 Chan TC, Wang YM, Yu M, *et al*. Comparison of corneal dynamic parameters and tomographic measurements using Scheimpflug imaging in keratoconus. *Br J Ophthalmol* 2018;102(1):42-47.

26 Ren SW, Xu LY, Fan Q, *et al*. Accuracy of new Corvis ST parameters for detecting subclinical and clinical keratoconus eyes in a Chinese population. *Sci Rep* 2021;11(1):4962.

27 Ostadian F, Farrahi F, Mahdian Rad A. Comparison of corneal epithelial thickness map measured by spectral domain optical coherence tomography in healthy, subclinical and early keratoconus subjects. *Med Hypothesis Discov Innov Ophthalmol* 2019;8(2):85-91.

28 Heidari Z, Hashemi H, Mohammadpour M, *et al*. Evaluation of corneal topographic, tomographic and biomechanical indices for detecting clinical and subclinical keratoconus: a comprehensive three-device study. *Int J Ophthalmol* 2021;14(2):228-239.

29 Lu NJ, Elsheikh A, Rozema JJ, *et al*. Combining spectral-domain OCT and air-puff tonometry analysis to diagnose keratoconus. *J Refract Surg* 2022;38(6):374-380.

30 Salomão MQ, Hofling-Lima AL, Gomes Esporcatte LP, *et al*. The role of corneal biomechanics for the evaluation of ectasia patients. *Int J Environ Res Public Health* 2020;17(6):2113.

31 Ferreira-Mendes J, Lopes BT, Faria-Correia F, *et al*. Enhanced ectasia detection using corneal tomography and biomechanics. *Am J Ophthalmol* 2019;197:7-16.

32 Salman A, Mazzotta C, Kailani O, *et al*. Diagnostic accuracy of corneal and epithelial thickness map parameters to detect keratoconus and suspect keratoconus. *J Ophthalmol* 2023;2023:6677932.

33 Hashemi H, Khabazkhoob M, Pakzad R, *et al*. Pentacam accuracy in discriminating keratoconus from normal corneas: a diagnostic evaluation study. *Eye Contact Lens Sci Clin Pract* 2019;45(1):46-50.

34 Shiga S, Kojima T, Nishida T, *et al*. Evaluation of CorvisST biomechanical parameters and anterior segment optical coherence tomography for diagnosing forme fruste keratoconus. *Acta Ophthalmol* 2021;99(6):644-651.

35 Peña-García P, Peris-Martínez C, Abbouda A, *et al*. Detection of subclinical keratoconus through non-contact tonometry and the use of discriminant biomechanical functions. *J Biomech* 2016;49(3):353-363.

36 Saad A, Debellemanière G, Zeboulon P, *et al*. Discrimination between keratoconus, forme fruste keratoconus, and normal eyes using a novel OCT-based tomographer. *J Cataract Refract Surg* 2023;49(11):1092-1097.

37 Hashemi H, Doroodgar F, Niazi S, *et al*. Comparison of different corneal imaging modalities using artificial intelligence for diagnosis of keratoconus: a systematic review and meta-analysis. *Graefes Arch Clin Exp Ophthalmol* 2024;262(4):1017-1039.

38 Song P, Ren SW, Liu Y, *et al*. Detection of subclinical keratoconus using a novel combined tomographic and biomechanical model based on an automated decision tree. *Sci Rep* 2022;12(1):5316.

39 Atalay E, Özalp O, Erol MA, *et al*. A combined biomechanical and tomographic model for identifying cases of subclinical keratoconus. *Cornea* 2020;39(4):461-467.

40 Zhang H, Tian L, Guo LL, *et al*. Comprehensive evaluation of corneas from normal, forme fruste keratoconus and clinical keratoconus patients using morphological and biomechanical properties. *Int Ophthalmol* 2021;41(4):1247-1259.

41 Hashemi H, Beiranvand A, Yekta A, *et al*. Pentacam top indices for diagnosing subclinical and definite keratoconus. *J Curr Ophthalmol* 2016;28(1):21-26.

42 Zhang XY, Ding L, Sun L, *et al*. Prognostic nomograms predicting risk of keratoconus in very asymmetric ectasia: combined corneal tomographic and biomechanical assessments. *Front Bioeng Biotechnol* 2022;10:839545.

43 Wallace HB, Vellara HR, Gokul A, *et al*. Comparison of ectasia detection in early keratoconus using scheimpflug-based corneal tomography and biomechanical assessments. *Cornea* 2023;42(12):1528-1535.

44 Vandevenne MM, Favuzza E, Veta M, *et al*. Artificial intelligence for detecting keratoconus. *Cochrane Database Syst Rev* 2023;11(11):CD014911.